ARTICLE

Synthesis of Triaxial $LiFePO_4$ Nanowire with a VGCF Core Column and a Carbon Shell through the Electrospinning Method

Eiji Hosono,[†] Yonggang Wang,[†] Noriyuki Kida,[‡] Masaya Enomoto,[‡] Norimichi Kojima,[‡] Masashi Okubo,[†] Hirofumi Matsuda,[†] Yoshiyasu Saito,[†] Tetsuichi Kudo,[†] Itaru Honma,[†] and Haoshen Zhou*[,†]

Energy Technology Research Institute, National Institute of Advanced Industrial Science and Technology, Umezono, 1-1-1, Tsukuba, 305-8568, Japan, Graduate School of Arts and Sciences, The University of Tokyo, Meguro-ku, Tokyo 153-8902, Japan

ABSTRACT A triaxial $LiFePO_4$ nanowire with a multi wall carbon nanotube (VGCF:Vapor-grown carbon fiber) core column and an outer shell of amorphous carbon was successfully synthesized through the electrospinning method. The carbon nanotube core oriented in the direction of the wire played an important role in the conduction of electrons during the charge−discharge process, whereas the outer amorphous carbon shell suppressed the oxidation of Fe^{2+}. An electrode with uniformly dispersed carbon and active materials was easily fabricated via a single process by heating after the electrospinning method is applied. Mössbauer spectroscopy for the nanowire showed a broadening of the line width, indicating a disordered coordination environment of the Fe ion near the surface. The electrospinning method was proven to be suitable for the fabrication of a triaxial nanostructure.

KEYWORDS: $LiFePO_4$ • nanowires • electrospinning method • lithium ion battery • positive materials • nanostructure control

INTRODUCTION

The electrospinning method has recently been the focus of scientific attention since nanowires can be easily obtained through a simple mechanism (1, 2). First, a polymer solution is placed on the tip of a needle. When the electric potential reaches a critical level, the electrostatic force causes the drawing out of a fine jet of solution, which includes long polymer chains. The jet then whips toward the grounded target and creates dry nanowires through the drying of the solvent during the electrospinning process between the needle and the target. The nanowires are collected on the target.

Although there have been many reports on the synthesis of polymer nanowire by the electrospinning method (1−5), the synthesis of metal oxide nanowires (6−9) by the electrospinning method is only now being intensively investigated because metal oxide nanowires can also be obtained by using a polymer solution including metal salts and metal alkoxide, as in the case of sol−gel methods (6−9).

If nanowires such as carbon nanotube and metal nanowire are dispersed into a polymer solution including metal salts, metal oxide nanowires with a core, which is oriented in a one-dimensional direction, will be obtained. It is our finding that we can easily fabricate core/shell nanowires with different properties through the selection of the core materials and shell materials.

For example, $LiFePO_4$ is an important candidate for an alternative positive electrode of $LiCoO_2$ for a lithium ion battery (10−14). However, the low electron conduction in $LiFePO_4$ is a major obstacle, especially to rapid Li-ion intercalation/deintercalation. To overcome this problem, one must intensively investigate the carbon coating technique as a means to introduce an electron path (15−17).

A composite nanowire of $LiFePO_4$ and carbon could be obtained by the electrospinning method using a polymer solution that includes Li, Fe, and P sources because the polymer is easily converted into amorphous carbon by heating under a reduction or in an inert atmosphere (17, 18). The carbon-coated $LiFePO_4$ is very important for the suppression of the oxidation of Fe^{2+} because the inhibition of oxidation causes good performances of lithium-ion battery (19). Therefore, the electrospinning method is suitable for the synthesis of the composite material between $LiFePO_4$ and amorphous carbon. However, the conductivity of the amorphous carbon is lower than that of graphite and not sufficient for the high-rate lithium-ion battery for the electric vehicle, which needs large current density (20, 21). If the heating temperature were to be increased to obtain graphite, $LiFePO_4$ would be decomposed. Therefore, another electron conduction path must also be introduced.

In this work, we report on a carbon/$LiFePO_4$/multiwall carbon nanotube (VGCF) nanowire with a triaxial structure; to the best of our knowledge, this is the first report of its kind. The triaxial structure, which contains the VGCF core column, the composite of $LiFePO_4$/amourphous carbon, and an outer

* Corresponding author. E-mail: hs.zhou@aist.go.jp.
Received for review September 29, 2009 and accepted December 5, 2009
[†] National Institute of Advanced Industrial Science and Technology.
[‡] The University of Tokyo.
DOI: 10.1021/am900656y

Published on Web 12/16/2009

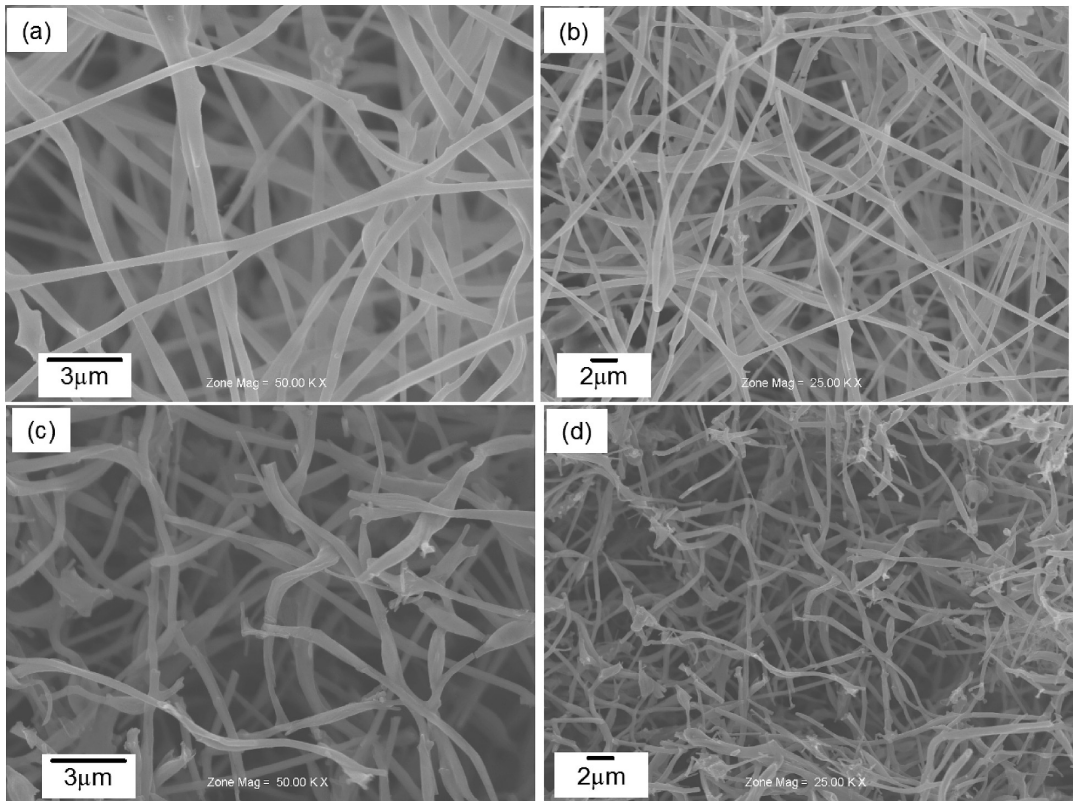

FIGURE 1. FE-SEM images of (a, b) the dried materials and (c, d) the materials heated at 800 °C for 10 h, respectively. The precursor solution is made of poly acryl acid, the sources of Li, Fe, P, and VGCF.

amorphous carbon shell, is needed for an effective lithium-ion battery with high current density. This is because the carbon nanotube core oriented along the direction of the wire plays an important role in the conduction of electrons during the charge–discharge process, whereas the outer amorphous carbon shell suppresses the oxidation of Fe^{2+}. Moreover, electrodes with uniformly dispersed carbon and active materials are easily fabricated via a single process by heating after the electrospinning method. The electrospinning method is a powerful technique for designing the desired nanostructure.

EXPERIMENTAL SECTION

First, the $LiNO_3$ (0.2 M), $Fe(NO_3)_3 \cdot 9H_2O$ (0.2 M), $NH_4H_2PO_4$ (0.2 M), and 0.8 g of poly acrylic acid (MW:250000) were dissolved into a mixed solution of methanol (10 mL)/water (9 mL)/ HNO_3 (1 mL). Second, 0.2 g of VGCF (multiwall carbon nanotube, SHOWA DENKO) was ultrasonically dispersed into the solution using a sono-horn. The resultant precursor solution was poured into a syringe connected to a metal needle. A direct-current electric field of 25 kV was applied between the needle and the Al foil target used for collection. The as-spun materials were then dried overnight in a vacuum at 100 °C. Finally, the dried materials that were separated from the Al foil were heated at 800 °C for 10 h under Ar flow conditions. For purposes of comparison, conventional bulk $LiFePO_4$ was synthesized by heating a mixture of CH_3COOLi, $FeC_2O_4 \cdot 2H_2O$, and $NH_4H_2PO_4$ at 700 °C for 10 h in an Ar flow (5% : H_2).

The crystal structure was identified using X-ray diffraction (XRD) analysis with a Bruker AXS D8 Advance using Cu Kα radiation. The morphology was observed by means of field-emission scanning electron microscopy (FESEM) and high-resolution transmission electron microscopy (HRTEM) using a Carl Zeiss Gemini Supra and a JEOL JEM-2010F, respectively. Raman spectra were recorded in backward geometry on a NIHON BUNKO Ventuno spectrometer (NSR-1000DT) at room temperature; the powder samples were excited using the 632.8 nm wavelength line from a He–Ne laser. The thermal behavior of the samples was examined by thermogravimetry-differential thermal analysis (TG-DTA) with a Mac Science 2020S analyzer using a heating rate of 10 °C/min in air. For the ^{57}Fe Mössbauer spectroscopy, ^{57}Co in Rh was used as a Mössbauer source. The spectra were calibrated by using the six lines of a body-centered cubic iron foil (α-Fe) whose center was taken as a zero isomer shift. The line fit was carried out by least-squares fitting with a Lorentzian line shape.

Electrochemical measurements were taken by a three-electrode cell. The triaxial $LiFePO_4$ nanowires were mixed and ground with 5 wt % Teflon powder. The mixture was spread and pressed on the SUS-304 mesh, which was used as the working electrode. The reference and counter electrode were prepared by lithium metals on SUS-304 mesh. A 1 mol dm^{-3} $LiClO_4$ in EC/DEC was used as an electrolyte. Cell assembly was carried out in a glovebox in an argon atmosphere. The weight in specific capacity (mA h/g) and current rate were calculated only for active materials.

RESULTS AND DISCUSSION

Figure 1a–d shows FE-SEM images of the dried compound and the compound heated for 10 h at 800 °C for 10 h. As shown in images c and d in Figure 1, the nanowire structure of the dried compound in images a and b in Figure 1 is maintained, even if the sample was heated for 10 h at 800 °C. The nonwoven fabric morphology constructed by the nanowire, as shown in Figure 1, suppresses the aggregation and grain growth to micrometer scale grain at a high temperature. Even in the high-magnification images a and

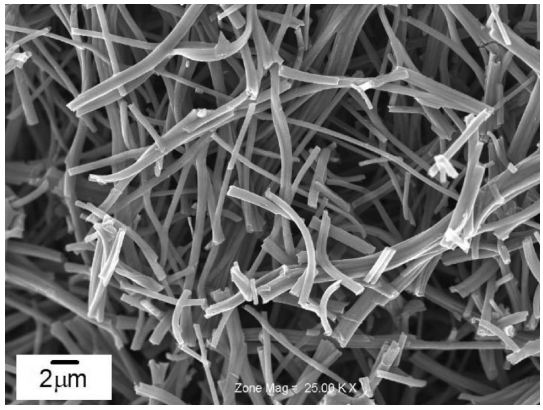

FIGURE 2. FE-SEM images of the materials heated at 800 °C for 10 h. The precursor solution includes the poly acryl acid, and the sources of Li, Fe, and P without VGCF.

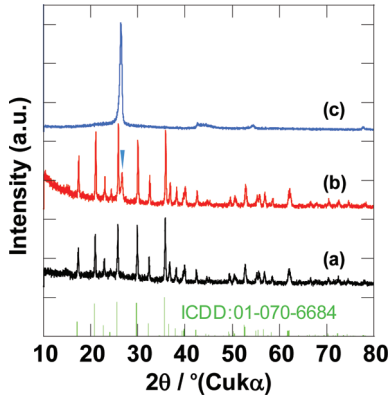

FIGURE 3. XRD patterns of (a) the nanowire without VGCF after heating, (b) the nanowire with VGCF after heating, and (c) only VGCF.

c in Figure 1, VGCF could hardly be observed. Thus, almost all the VGCF is incorporated into the spun nanowire as the core; this is one of the advantages of the electrospinning method. By the dispersion of VGCF into the polymer solution with the Li, Fe, P sources, the VGCF was oriented in the direction of the polymer nanowires (22−24). When the precursor solution without VGCF was treated according to the same procedure, a similar nanowire structure was obtained, which is shown in Figure 2 for purposes of comparison.

Figure 3 shows the XRD patterns of the nanowire without VGCF after heating (a), the nanowire with VGCF after heating (b), and only VGCF (c). Both the XRD patterns of (a) and (b) correspond to the patterns of the $LiFePO_4$ (ICDD: 01−070−6684) and VGCF (Figure 3(c)) without any impurity phase. Frequently, the $LiFePO_4$ obtained by the heating procedure of the sol−gel method includes other phases such as Fe_2O_3 or Fe_2P (10, 25). In this work, however, pure $LiFePO_4$ was obtained by the electrospinning method, as can be deduced from the XRD pattern.

Generally, for a carbon compound, the ratio of the G-band to the D-band in the Raman spectrum is a good means of estimating the concentration of defects. The D-band at about 1300 cm^{-1} and the G-band at about 1580 cm^{-1} are ascribed to disorder such as defects, and the E_{2g} mode of graphite, respectively (26). The peak intensity of the G-band becomes

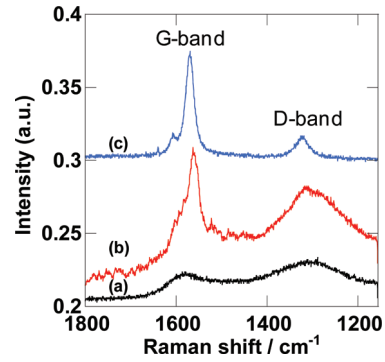

FIGURE 4. Raman spectra of (a) the $LiFePO_4$ nanowire without VGCF after heating, (b) the $LiFePO_4$ nanowire with VGCF after heating, and (c) only VGCF.

strong as there is a decrease in defect concentration. We could therefore distinguish between amorphous carbon, and highly crystalline carbon like VGCF, by means of Raman spectroscopy. Figure 4a−c shows the Raman spectra of the $LiFePO_4$ nanowire without VGCF after heating, the $LiFePO_4$ nanowire with VGCF after heating, and VGCF, respectively. All spectra show the D-band and G-band of the carbon materials, although the ratio of the G/D-bands is different. The line width in Figure 4a is rather broad, and the intensity of the D-band is higher than that of the G-band. In contrast, the spectrum for VGCF (Figure 4c) shows a strong peak of the G-band with a narrow line width, and a weak peak of the D-band, which indicates the presence of highly crystalline VGCF, whereas the spectrum with the weak G-band and the strong D-band in Figure 4a indicates the amorphous carbon obtained by heating the poly acrylic acid. Concerning spectrum b, both a broad and a sharp peak in the region of the G-band were observed. This indicates that the compound that was synthesized through the electrospinning method using a precursor containing VGCF consists of $LiFePO_4$, VGCF, and amorphous carbon.

Figure 5 shows TEM images of the $LiFePO_4$/amorphous carbon nanowire with VGCF obtained thorough the electrospinning method. Figure 5a is a low-magnification image of the nanowire. Figure 5b shows the magnified part in a. The core nanowire and the surrounding thin shell are observable in both images. Figure 5c shows the magnified part of the core nanowire in b. The inset image, which is the electron diffraction pattern of the core nanowire, shows two clear spots perpendicular to the nanowire direction due to the interlamellar distance of the graphene layers in VGCF. The lattice image indicates a similar interlamellar distance of 3.4 Å, as shown in Figure 5d. Taking into account images c and d, the core nanowire could be ascribed to VGCF. Magnified parts of the shell are shown in images e and f in Figure 5. The electron diffraction pattern of the inset in Figure 5e agrees with the pattern of the $LiFePO_4$. The dark part and the white part in Figure 5e could most likely be ascribed to $LiFePO_4$ and amorphous carbon, respectively. In fact, the high-magnification image of the interface part in Figure 5f shows a lattice fringe between the $LiFePO_4$ (111) and the amorphous carbon. The surface of the $LiFePO_4$ shell thus seems to be coated with amorphous carbon.

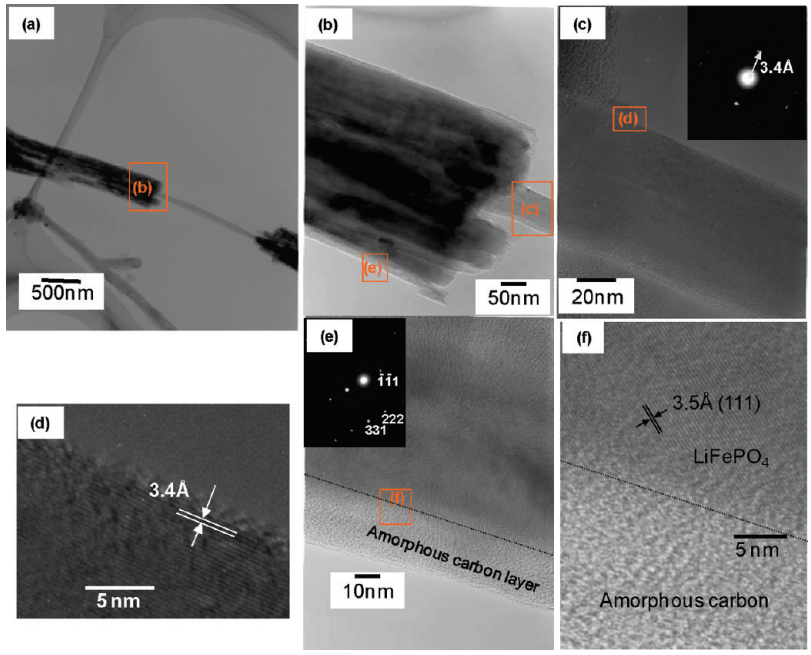

FIGURE 5. TEM images of the $LiFePO_4$/amorphous carbon nanowire with VGCF obtained thorough the electrospinning method. (a) Low-magnification image of the nanowire. (b) Magnified part in a. (c) Magnified part of the fine nanowire in b. The inset image shows an electron diffraction pattern of the fine nanowire. (d) Lattice image in c. (e, f) Parts of the shell.

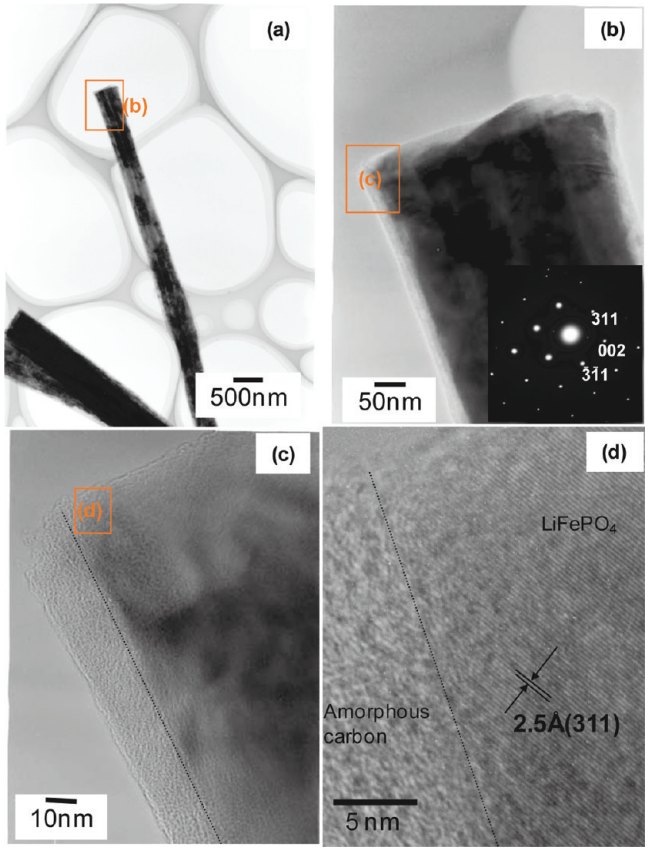

FIGURE 6. TEM images of the $LiFePO_4$ nanowire without VGCF. (a) Low-magnification image of the $LiFePO_4$ nanowire without VGCF. (b, c) Images of the outer shell. (d) Outer/inner shell's interface.

When the $LiFePO_4$ nanowire without VGCF (Figure 2) was fabricated, nanowires as shown in Figure 6 were observed. Figure 6a is a low-magnification image of an $LiFePO_4$ nanowire without VGCF. The images in b and c indicate that the

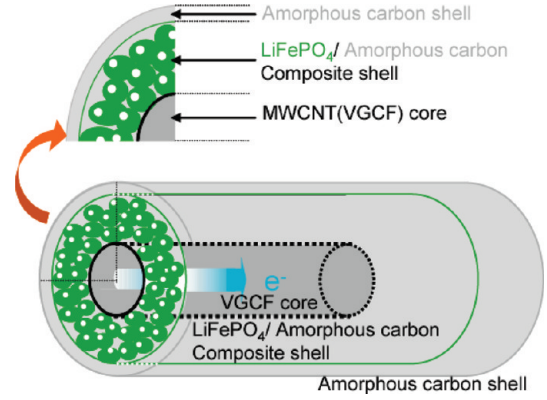

FIGURE 7. Model image of the triaxial nanowire with a VGCF core column, and the two layer shells: an outer shell of amorphous carbon, and an inner composite shell of $LiFePO_4$ and amorphous carbon.

outer shell is coated with amorphous carbon, which is the white part, and that the inner shell is a composite of $LiFePO_4$ and amorphous carbon. Figure 6 d shows the outer/inner shell interface and displays the lattice fringe between the $LiFePO_4$ (311) and the amorphous carbon. By applying the electrospinning method, we easily synthesized a composite nanowire of $LiFePO_4$ coated with a layer of amorphous carbon.

Figure 7 shows a model image of the triaxial nanowire consisting of a VGCF core column, an $LiFePO_4$/amorphous carbon composite shell, and the outer amorphous carbon surface.

To clarify the coordination environment around Fe^{2+} in the $LiFePO_4$ nanowire, we performed ^{57}Fe Mössbauer spectroscopy. Figure 8a represents the Mössbauer spectrum for a triaxial $LiFePO_4$ nanowire at room temperature. For comparison, the spectrum for bulk $LiFePO_4$ without a carbon coating is also shown, in Figure 8b.

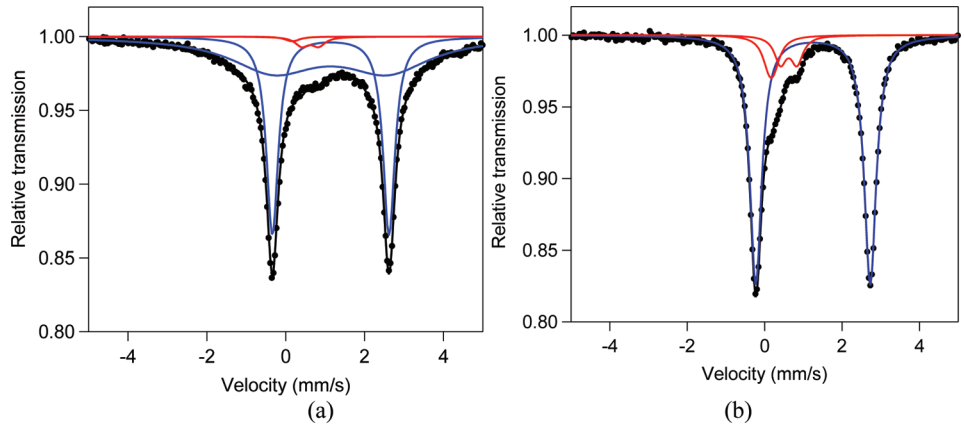

FIGURE 8. ^{57}Fe Mössbauer spectra for (a) $LiFePO_4$ triaxial nanowire with VGCF, (b) bulk $LiFePO_4$ at room temperature.

Table 1. ^{57}Fe Mössbauer Parameters of $LiFePO_4$ Triaxial Nanowires with VGCF and Bulk $LiFePO_4$

		IS (mm/s)	QS (mm/s)	Γ (mm/s)	fraction (%)
bulk LiFePO4	Fe(II) (S = 2)	1.25	2.96	0.37	82.4
	Fe_2P (I)	**0.62**[a]	**0.427**[a]	0.36	9
	Fe_2P (II)	**0.17**[a]	**0.12**[a]	0.4	8.6
core/shell	Fe(II) (S = 2)	**1.14**[b]	2.96	0.36	43.9
LiFePO4 nanowire	Fe(II) (S = 2)	**1.14**[b]	2.89	2.62	53.2
	Fe_2P (I)	**0.62**[a]	**0.427**[a]	0.4	2.2
	Fe_2P (II)	**0.17**[a]	**0.12**[a]	0.4	0.6

[a] Constant values. [b] Restricted to be the same value.

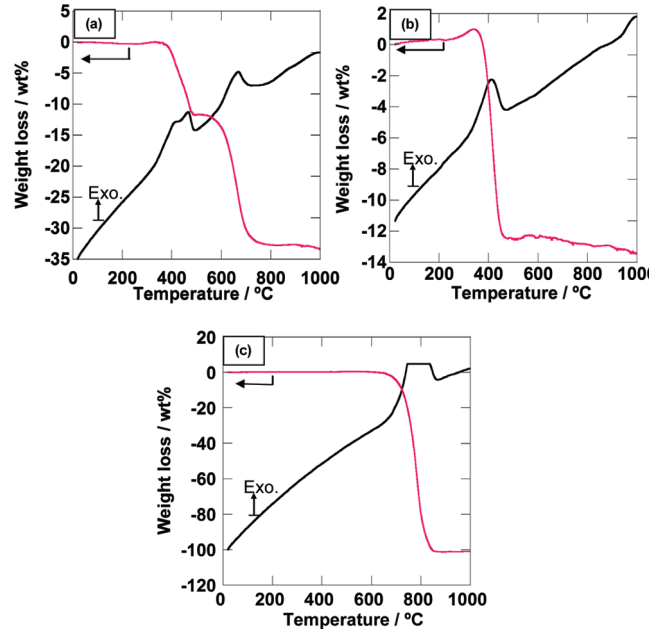

FIGURE 9. TG-DTA measurement of (a) $LiFePO_4$ triaxial nanowires with VGCF, (b) $LiFePO_4$ nanowires without VGCF, and (c) only VGCF.

Concerning bulk $LiFePO_4$, the spectrum was fitted with one major doublet and two minor doublets. The fitting parameters are summarized in Table 1. The dominant doublet (blue line in Figure 8b) had an isomer shift (IS) = 1.25 mm/s and a quadrupole splitting (QS) = 2.96 mm/s, which are typical for octahedral high spin Fe^{2+} in $LiFePO_4$ (27). The other minor doublets (red lines in Figure 8 b) indicate the presence of impurities, most likely Fe_2P (28). These three doublets reproduced the results of our experiment well, and are in substantial agreement with results in the literature (27, 28).

In contrast, the best fit for the spectrum for triaxial $LiFePO_4$ nanowire was obtained with four doublets, i.e., two major doublets (blue lines in Figure 8a), and two minor doublets (red lines in Figure 8a). On the basis of the IS and QS values in Table 1, both the major doublets should be attributed to the Fe^{2+} in $LiFePO_4$. However, one of the two doublets has a quite broad line width of 2.62 mm/s. It should also be noted that the molar fraction for the broad doublet exceeds 50% within the sample.

Generally, the broadening of the Mössbauer spectrum suggests a disordered coordination environment. In this regard, Kuwano et al. reported that a ball-milled Cr−Fe alloy showed a pronounced broadening of the spectrum as the milling proceeded, i.e., the crystallite size decreased (29). By the same principle, because a triaxial $LiFePO_4$ nanowire contains a smaller crystallite size and larger surface area than one with bulk $LiFePO_4$, the additional broad doublet for the triaxial $LiFePO_4$ nanowire could be explained by the disordered coordination environment around Fe^{2+} near the surface.

Furthermore, it should be noted that cation mixing between Li-ion and Fe-ion frequently occurs in $LiFePO_4$ (30). Thus, structural disorder due to cation mixing could also be the origin of the disordered coordination environment around the Fe-ion, which produced the broad spectrum. Although the molar fraction of cation mixing does not normally exceed 10%, it could provide another reason for the broad Mössbauer spectrum for the triaxial $LiFePO_4$ nanowire.

TG-DTA measurement in an air condition was carried out in order to estimate the weight percentage of the active material in the $LiFePO_4$ nanowire with VGCF, and without VGCF, as shown in panels a and b in Figure 9, respectively. The weight loss and exothermic, which peaks around 400−500 °C in Figure 9a, correspond to the decomposition of $LiFePO_4$ and the amorphous carbon, as can be inferred from the TG-DTA curves for the nanowires without VGCF in Figure 9b. The weight loss and exothermic, which peaks

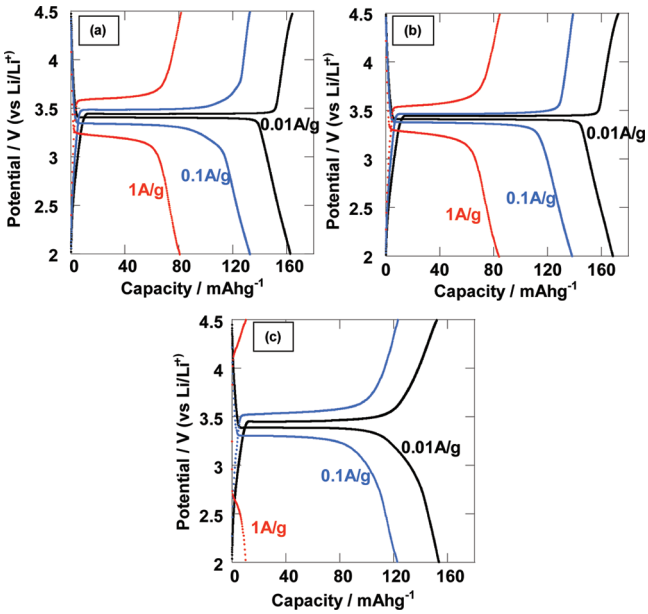

FIGURE 10. Charge/discharge curves of (a) the 10th cycle by the triaxial nanowires of $LiFePO_4$ with VGCF core column, (b) the triaxial nanowires of $LiFePO_4$ to which additional carbon (acetylene black) has been added, and (c) the $LiFePO_4$ nanowires without VGCF core column to which additional carbon such as acetylene black has not been added.

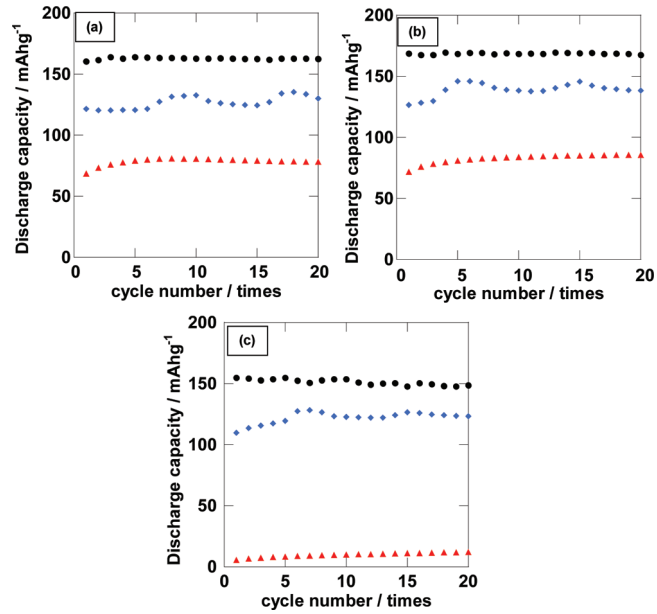

FIGURE 11. Performance cycles of (a) triaxial nanowires of $LiFePO_4$ with a VGCF core column, (b) triaxial nanowires of $LiFePO_4$ to which additional carbon (acetylene black) has been added, and (c) $LiFePO_4$ nanowires without a VGCF core column to which additional carbon such as acetylene black has not been added.

around 600−800 °C in Figure 9a, are due to the decomposition of the VGCF, as shown in Figure 9c. The weight loss in panels a and b in Figure 9 indicates that the carbon ratios of nanowire with and without VGCF are 33.26 and 13.45 wt %, respectively.

Figure 10 shows the charge/discharge curves of the 10th cycle by the electrode using triaxial nanowires of $LiFePO_4$ with a VGCF core column (a), the triaxial nanowires of $LiFePO_4$ with additional carbon (acetylene black) (b), and the $LiFePO_4$ nanowires without a VGCF core column to which additional carbon such as acetylene black has not been added (c). The additional carbon is mixed by hand mixing in a mortar. The ratios of the active materials ($LiFePO_4$) of a−c are 63.4, 50, and 82.2 wt %, respectively. Cathode performance was tested at three charge/discharge rates (0.01, 0.1, and 1). Panels a and b in Figure 10 suggest that the charge/discharge capacity for the electrode using triaxial nanowires of $LiFePO_4$ with a VGCF core column without acetylene black (a) and with acetylene black (b). Both samples indicated a similar capacity of around 160, 130, and 80 mA h/g at current densities of 0.01, 0.1, and 1 A/g, respectively. Because the theoretical capacity of $LiFePO_4$ is around 170 mA/g, the electrode using triaxial nanowire could perform quite well under low current density conditions. When the current density was increased to 0.1 and 1 A/g, the capacity without acetylene black (a) and with acetylene black (b) decreased in a similar manner. This result indicated that the addition of other electroconductive material does not affect the performance of the electrode for a lithium ion battery. However, the high rate of performance at 1 A/g is not particularly favorable. We confirmed the electrode on the SUS mesh in the SEM image (see the Supporting Information, Figure S1). The triaxial nanowire structure was damaged by the grinding process for mixing with Teflon powder. Therefore, the improvement of the fabrication process for the electrodes will improve properties in regard to high current density. Furthermore, the charge/discharge curves generated by the electrode using $LiFePO_4$ nanowires without a VGCF core column (c) were rather different. In the case of a low current density such as 0.01 and 0.1 A/g, the capacity was similar to that of an electrode using triaxial nanowires of $LiFePO_4$ with a VGCF core column. However, when the current density was increased up to 1 A/g, the capacity was reduced significantly. This proved that the VGCF is indispensable as a current collector at a high current density, while the amorphous carbon could serve as a current collector at a low current density. In this study, we have seen that the special nanostructure of triaxial nanowires with a VGCF core and two layer shells (an outer shell of amorphous carbon, and an inner composite shell of $LiFePO_4$ and amorphous carbon) is damaged by the process of mixing to prepare the electrode on the SUS mesh. However, the uniformly dispersed VGCF as a current collector, and the composite shell of $LiFePO_4$ and amorphous carbon, are easily obtained via a single process by heating after the electrospinning method has been applied. In short, electrodes with uniformly dispersed carbon and active materials are easily fabricated. This is one of the important reasons for employing the electrospinning method for the fabrication of electrodes. Figure 11 shows the performance cycle of an electrode using triaxial nanowire of $LiFePO_4$ with a VGCF core column (a), triaxial nanowires of $LiFePO_4$ to which additional carbon (acetylene black) is added (b), and $LiFePO_4$ nanowires without a VGCF core column to which additional carbon such as acetylene black has not been added (c). The nanowires with an outer shell based on amorphous carbon, which is easily fabricated by the heating

via the electrospinning method, could show a positive performance cycle without any degradation in capacity.

CONCLUSIONS

The electrospinning method could be used to fabricate triaxial $LiFePO_4$ nanowire with a VGCF core column and two layer shells, with an outer shell of amorphous carbon, and an inner composite shell of $LiFePO_4$ and amorphous carbon. Electrodes with uniformly dispersed carbon and active materials are easily fabricated by a single process of heating after employment of the electrospinning method. Our study leads us to believe that the VGCF core column and outer amorphous carbon surface play an important role in forming an electron conduction path and inhibiting the oxidation of Fe^{2+}. The electrospinning method is a powerful technique to design complicated nanostructures such as triaxial nanowires.

Supporting Information Available: SEM images of the electrode on the SUS mesh (PDF). This material is available free of charge via the Internet at http://pubs.acs.org.

REFERENCES AND NOTES

(1) Kameoka, J.; Czaplewski, D.; Liu, H.; Craighead, H. G. *J. Mater. Chem.* **2004**, *14*, 1503.
(2) Sell, S. A.; Bowlin, G. L. *J. Mater. Chem.* **2008**, *18*, 260.
(3) Choi, S. W.; Jo, S. M.; Lee, W. S.; Kim, Y. R. *Adv. Mater.* **2003**, *15*, 2027.
(4) Choi, S. W.; Kim, J. R.; Ahn, Y. R.; Jo, S. M.; Cairns, E. J. *Chem. Mater.* **2007**, *19*, 104.
(5) Li, D.; Ouyang, G.; McCann, J. T.; Xia, Y. *Nano Lett.* **2005**, *5*, 913. 2005.
(6) Kim, I. D.; Hong, J. M.; Lee, B. H.; Kim, D. Y.; E. Jeon, K.; Choi, D. K.; Yang, D. J. *Appl. Phys. Lett.* **2007**, *91*, 163109.
(7) Gu, Y.; Chen, D.; Jiao, X.; Liu, F. *J. Mater. Chem.* **2007**, *17*, 1769.
(8) Kumar, A.; Jose, R.; Fujihara, K.; Wang, J.; Ramarkrishna, S. *Chem. Mater.* **2007**, *19*, 6536.
(9) Ding, B.; Ogawa, T.; Kim, J.; Fujimoto, K.; Shiratori, S. *Thin Solid Films* **2008**, *516*, 2495.
(10) Shiraishi, K.; Dokko, K.; Kanamura, K. *J. Power Sources* **2005**, *146*, 555.
(11) Laffont, L.; Delacourt, C.; Gibot, P.; Wu, M. Y.; Kooyman, P.; Masquelieer, C.; Tarascon, J. M. *Chem. Mater.* **2006**, *18*, 5520.
(12) Wang, Y.; Wang, J.; Yang, J.; Nuli, Y. *Adv. Funct. Mater.* **2006**, *16*, 2135.
(13) Ravet, N.; Gauthier, M.; Zaghib, K.; Goodenough, J. B.; Mauger, A.; Gendron, F.; Julien, C. M. *Chem. Mater.* **2007**, *19*, 2595.
(14) Wang, Y. G.; Wang, Y. R.; Hosono, E.; Wang, K. X.; Zhou, H. S. *Angew. Chem., Int. Ed.* **2008**, *47*, 7461.
(15) Sides, C. R.; Croce, F.; Young, V. Y.; Martin, C. R.; Scrosati, B. *Electrochem. Solid-State Lett.* **2005**, *8*, A484.
(16) Gabrisch, H.; Wilcox, J. D.; Doeff, M. M. *Electrochem. Solid-State Lett.* **2006**, *9*, A360.
(17) Kim, C.; Yang, K. S.; Kojima, M.; Yoshida, K.; Kim, Y. J.; Kim, Y. A.; Endo, M. *Adv. Funct. Mater.* **2006**, *16*, 2393.
(18) Wang, L.; Yu, Y.; Chen, P. C.; Chen, C. H. *Scr. Mater.* **2008**, *58*, 405.
(19) Sisbandini, C.; Brandell, D.; Gustafsson, T.; Nyholm, L. *J. Electrochem. Soc.* **2009**, *156*, A720.
(20) Zhou, H. S.; Li, D.; Hibino, M.; Honma, I. *Angew. Chem., Int. Ed.* **2005**, *44*, 797.
(21) Moriguchi, I.; Hidaka, R.; Yamada, H.; Kudo, T.; Murakami, H.; Nakashima, N. *Adv. Mater.* **2006**, *18*, 69.
(22) Sung, J. H.; Kim, H. S.; Jin, H. J.; Choi, H. J.; Chin, I. J. *Macromolecules* **2004**, *37*, 9899.
(23) Xie, X. L.; Mai, Y. W.; Zhou, X. P. *Mater. Sci. Eng., R* **2005**, *49*, 89.
(24) Aryal, S.; Kim, C. K.; Kim, K. W.; Khil, M. S.; Kim, H. Y. *Mater. Sci. Eng., C* **2008**, *28*, 75.
(25) Rho, Y. H.; Nazar, L. F.; Perry, L.; Ryan, D. *J. Electrochem. Soc.* **2007**, *154*, A283.
(26) Kurita, S.; Yoshimura, A.; Kawamoto, H.; Uchida, T.; Kojima, K.; Tachibana, M.; Morales, P. M.; Nakai, H. *J. Appl. Phys.* **2005**, *97*, 104320.
(27) Hannoyer, B.; Prince, A. A. M.; Jean, M.; Liu, R. S.; Wang, G. X. *Hyperfine Interact.* **2006**, *167*, 767.
(28) Rho, Y.-H.; Nazar, L. F.; Perry, L.; Ryan, D. *J. Electrochem. Soc.* **2007**, *154*, A283.
(29) Kuwano, H.; Ouyang, H.; Fultz, B. *Nanostruct. Mater.* **1992**, *1*, 143.
(30) Yang, S.; Song, Y.; Zavalij, P. Y.; Whittingham, M. S. *Electrochem. Commun.* **2002**, *4*, 239.

AM900656Y